Journal of Environmental Chemical Engineering 13 (2025) 115010

Contents lists available at ScienceDirect

Journal of Environmental Chemical Engineering

journal homepage: www.elsevier.com/locate/jece

Continuous electrophoretic separation of submicron-microplastics from freshwater

Jui-Yen Lin [a,b,*], Cuijuan Feng [b], Ingyu Lee [c], Hyunook Kim [c], Chin-Pao Huang [b]

[a] Department of Chemical and Materials Engineering, National Kaohsiung University of Science and Technology, Kaohsiung City 807, Taiwan
[b] Department of Civil and Environmental Engineering, University of Delaware, Newark, DE 19702, USA
[c] Department of Environmental Engineering, University of Seoul, Seoul 02504, South Korea

ARTICLE INFO

Keywords:
Nanoplastics
Electrophoresis
Electrofiltration
Zeta potential
PS latex
Clean water and sanitation

ABSTRACT

Anthropogenic and natural weathering processes have produced submicron microplastics (MPs), an emerging contaminant. Due to small size, the treatment of submicron plastics particles by membrane processes requires small cutoff membranes, which necessitates great pressure gradient and suffers from clogging. The present study aims to develop an electrophoretic separation system for the separation of negatively charged submicron plastics particles from water. An electric field was supplied to produce an electrostatic force to counter the drag force in the permeation stream, thereby, preventing submicron plastics particles from entering the permeate. The critical electric field (E_c) for complete particles removal was estimated based on the dilute-to-influent flow rate ratio (q_d), zeta potential, and size of submicron plastics particles. The result showed that at steady-state, particle removal could reach 99 % at $E > E_c$ at $q_d = 0.5$. The distribution of plastics particles during electrophoretic separation was analyzed considering electrophoresis and particle deposition. The particle removal efficiency can be modelled by hydraulic condition and critical electric field. Finally, the engineering aspects such as long-term operation, electrode degradation and influence of coexisted constituents were evaluated. The operation cost of electrophoretic separation was calculated to be USD 0.48/m^3, which is cost-effective at small scales compared to conventional membrane processes.

1. Introduction

The widespread use of plastics in modern society has led to the emergence of plastics pollution because of high durability and low biodegradability. The annual production of plastics was 360 million tonne in 2018 and projected to grow to 1600 million tonne by 2050 [1]. At the present, only 6–26 % of plastics wastes are recycled and 21–42 % are landfilled, suggesting a large quantity of plastics flux into the aquatic environment [2]. Environmental stresses, such as UV light, mechanical abrasion, and biological interaction further fragmentate plastics debris to fine size, e.g., microplastics (MP, d < 5 mm) [3]. Extensive studies have revealed that MPs interferes with the ecosystem at a multi-magnitude level, including carbon circulation, habitant change, and bioaccumulation [4]. Recent advancement in analytical methods has enabled the detection of ultrafine plastics, specifically, in sub-micrometer size in the environment [5], which raises increasing concerns because of increase in specific surface area and nanotoxicity [6,7]. The mechanical stress incurred by pumping and impelling process in wastewater treatment plants (WWTPs) is one of the important sources of submicron plastics particles [8]. Enfrin et al. [3] have estimated that the total number of microplastics in the effluent of WWTPs double that in the influent. Furthermore, some MPs are manufactured intentionally for specific applications in scrubs, fillers, biomedical diagnosis and treatment [9]. These primary MPs are mostly made of polystyrene (PS) through suspension polymerization with size as small as 100 nm. Polystyrene particles have been commonly found in wastewater and the environment [10]. Therefore, it is of great importance to develop effective methods to remove ultrafine plastics from surface water and control the emission from WWTPs.

The removal efficiency of submicron plastics particles by conventional water treatment processes is still unclear because most studies were focused on larger MPs. Submicron plastics particles can be removed by particle-particle interaction in coagulation and size exclusion in membrane process. Zhang et al. have reported that more than

* Corresponding author at: Department of Chemical and Materials Engineering, National Kaohsiung University of Science and Technology, Kaohsiung City 807, Taiwan.
E-mail address: jytlin@nkust.edu.tw (J.-Y. Lin).

https://doi.org/10.1016/j.jece.2024.115010
Received 14 September 2024; Received in revised form 7 November 2024; Accepted 2 December 2024
Available online 3 December 2024

90 % of PS submicron particles are removed in 30 min by coagulation in the presence of polyaluminium chloride at 400 mg L^{-1} dosage by charge neutralization [11]. Ali et al. have reported that coagulative removal of submicron plastics particles is sensitive to water property, especially pH, salinity, and natural organic matters [12]. Like biosolids, plastics particle is hydrophobic, therefore, the sedimentation basin of conventional WWTPs has become the major sink of MPs. Frehland et al. [13] have tracked the flux of metal-doped submicron plastics particles (0.2 μm) in a pilot-scale WWTPs and found that at least 50–60 % of MPs end up in the biosolid. The retention of MPs in membrane bioreactor was superior than activated sludge reactor [14]. Low-pressure membrane processes, *i.e.*, ultrafiltration (UF) and microfiltration (MF), are capable of rejecting MPs as long as the membrane pore size is smaller than that of plastics particles [15]. The MPs fouling of UF membrane is irreversible and detrimental to water production. Enfrin et al. have demonstrated that water flux declined by 38 % after 48 h operation and backwash (using permeate) only restored 6 % of flux, suggesting the irreversibility of fouling by MPs [16].

The intrinsic negative surface charge of plastics can be harnessed to develop a separation strategy other than size exclusion and particle-particle interaction. Since the submicron plastics particles of major polymers are negatively charged [17], it is possible to separate submicron plastics particles by electrophoresis. For crossflow MF and UF that operate on size exclusion principle, electrophoresis can repel charged particles away from the membrane surface and retard cake formation thereby greatly minimizing flux decline. However, when dealing with submicron particles, electrofiltration becomes energy-intensive because additional energy is required for particle separation.

In contrast, the electrophoretic separation system offers a cost-effective and sustainable alternative for separating submicron plastics particles from water. Unlike crossflow MF, electrophoretic separation membrane can have pore size greater than that of particles in question, which can enhance transmembrane water velocity. In other words, the membrane functions as a water flow divider in electrophoretic separation while minimizes particles capture by membrane. The electric field is applied to mobilize charged particles against the transmembrane water velocity through electrophoresis. In theory, the particles can be completely retained in the concentrate chamber when electrophoretic velocity is greater than the transmembrane velocity. Other advantage of electrophoretic separation is that the pumping energy can be minimal, as the membrane pore size can be as large as 10 μm [18], enabling the allocation of more energy to particle separation by electrophoresis than overcoming membrane resistance due to fouling. This benefit would be especially realized when dealing with submicron particles. Lin et al. [18] and Sung et al. [19] have demonstrated the feasibility of electrophoretic separation of colloidal SiO_2 (d = 84 nm), Al_2O_3 (d = 200 nm), and natural occurring colloids (d = 300 nm) from water using polymeric membranes with pore size greater than 3 μm. Sung et al. have observed that the particle removal efficiency increases with electric field and that the critical electric field for achieving complete removal is comparable to the value calculated based on zeta potential and conductivity [19]. Lin et al. have calculated force balance exerted on a single particle for predicting the terminal velocity [18].

This study aims to develop an electrophoretic separation system for the removal of negatively charged submicron plastics particles from fresh water. PS latex, a major primary MP, has been used as model submicron plastics particles. The fundamentals of electrophoresis were applied to predict the movement of particles in the separation system, allowing the estimation of critical electric field required for complete particle removal. The steady-state removal efficiency of the electrophoretic separation system was evaluated under various operation conditions, including hydraulic property, electric field, particle size, and initial particle concentration. A model was developed to describe the distribution of submicron plastics particles in the concentrated and dilute streams during electrophoretic separation. Results enabled the prediction of removal efficiency as a function of electric field, hydraulic condition, and zeta potential. An economic analysis was conducted to address the advantage of electrophoretic separation system and its implication for the control of submicron plastics particles in water.

2. Methodology

2.1. Characterization of model submicron plastics particles

Polystyrene (PS) latex (purchased from Polysciences Inc. Warrington, Pennsylvania, U.S.A.) of different submicron size, i.e., 300 nm, 500 nm, and 1000 nm, was selected as the model submicron plastics particles. The hydrodynamic diameter and electrophoretic mobility of submicron plastics particles was determined by a Zetasizer (Nano-ZS, Malvern Panalytical, Worcestershire, U.K.). A 50-mL suspension of PS particles was prepared in DI water to yield a particle concentration of 5×10^{11} #/L with 10^{-3} M $NaClO_4$ as electrolyte. Fast titration method was used to measure the electrophoretic mobility of submicron plastics particles at different pH according to previous work [17]. Briefly, a predetermined amount of acid ($HClO_4$) or base (NaOH) was added to 50 mL of plastics particle suspension with 30 min of equilibrium time. Equilibrium pH was recorded and then an aliquot was withdrawn for electrophoretic mobility measurements at an applied voltage of 150 V. The process was repeated to cover a wide range of pH from 2 to 10.

2.2. Apparatus

The electrophoretic separation system was run in continuous mode using a customized electrophoretic separation cell as presented in Fig. 1a. Fig. S1 shows the sketch of the reactor. The reactor was built from Plexiglass 15 cm in height, 10 cm in length, and 4.6 cm in width. The separation cell has one inlet and two outlets. The two outlets, dilute and concentrate streams, are on two sides of the reactor and separated by a stainless-steel membrane with a cut-off size of 10 μm. The electrodes were made of #316 stainless steel with a mesh size of 16 × 16 and placed at the two sides of the separation chamber. The electrode on the side of influent and concentrate stream was an anode while the electrode on the side of dilute stream was a cathode. The distance between anode and membrane was 0.5 cm; the distance between cathode and membrane was around 0.1 cm. A spacer, being placed between anode and membrane, creates an area of 17.5 cm^2 (3.3 cm×5.3 cm) for permeation. Hence, the active separation zone of the electrophoretic separation system was 3.3 cm× 5.3 cm× 0.5 cm (8.75 cm^3).

The set-up of electrophoretic separation resembles that of cross-flow electrofiltration. The electrophoretic separation cell was positioned vertically. The influent containing certain concentration of submicron plastics particles flowed upwardly from the bottom of the cell using a peristaltic pump (Masterflex L/S Digital Drive Systems, Cole-Parmer Instrument LLC., Illinois, U.S.A.). The feed water flowed upward into the reactor and split into two streams – a concentrate stream that exited from the outlet on the same side as influent, and a dilute stream that permeated through the membrane and exited from another side of the cell. The presence of membrane ensured uniform horizontal water velocity passing through the membrane as dilute stream. A DC power supply (Model E861, Consort, Belgium) was used to charge the electrodes – anode at concentrate side and cathode at dilute side at predetermined voltage, preventing submicron plastics particles from entering the dilute stream. The flow rate distribution between the concentrate and the dilute stream was controlled by precision flow-adjustment valves (McMaster-Carr, Illinois, U.S.A.). To reduce the interference of gas bubbles generated from water electrolysis with flowrate control, bubble traps made from HDPE leakproof bottles (30 mL capacity, Thermo Fisher Scientific Inc., Maryland, U.S.A.) were installed at both outlets. The vertical configuration of the reactor facilitates the easy flushing of gases evolved from the electrodes out of the reactor into the bubble traps.

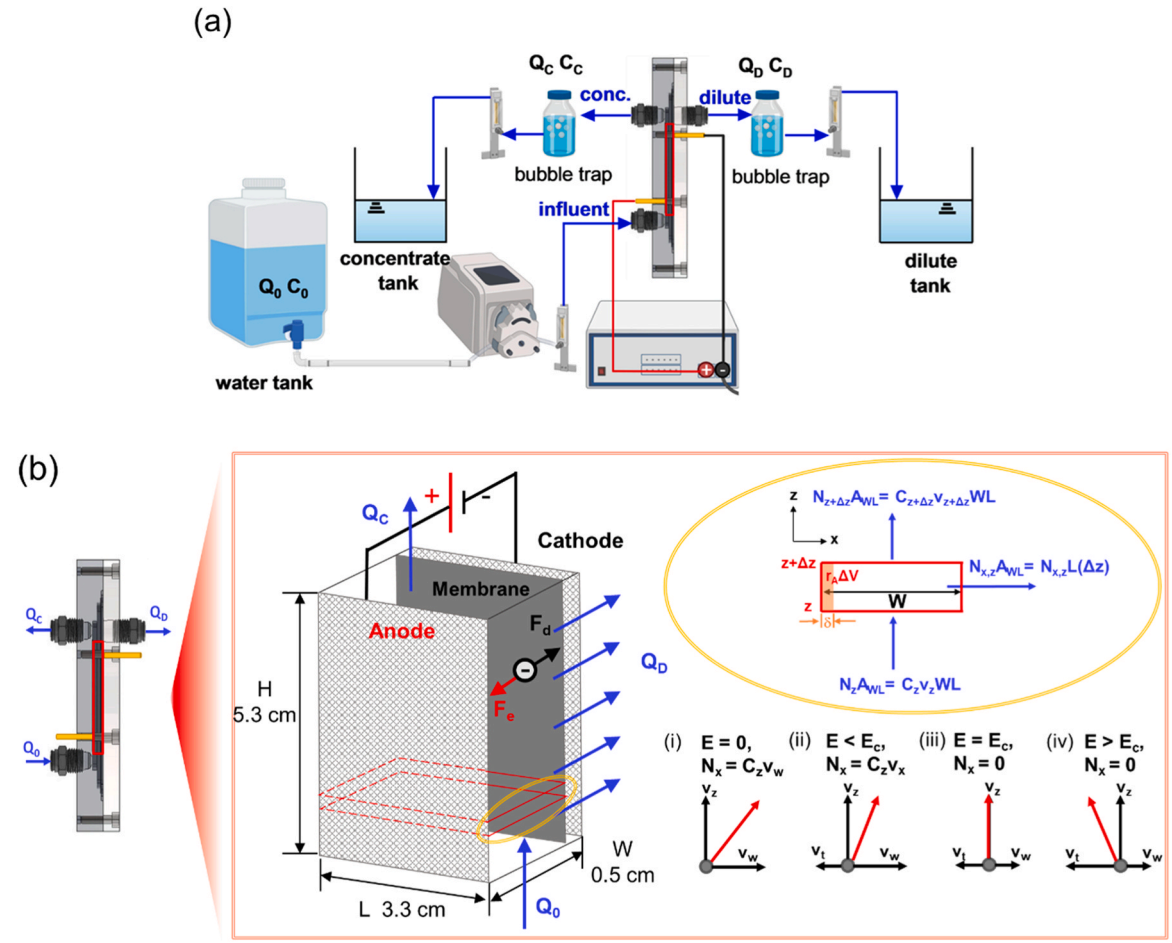

Fig. 1. (a) Experimental set-up of electrophoretic separation system. (b) Schematic illustration of the electrophoretic separation cell and movement of negatively-charged plastics particles in separation zone.

2.3. Experimental method

Prior to experiments, both electrodes and the membrane were cleaned with Sparkleen detergent (Thermo Fisher Scientific Inc., Maryland, U.S.A.), followed by thoroughly rinsing with DI water and absolute ethanol (200 proof, Lab Alley LLC., Texas, U.S.A.), and left to dry overnight. New electrodes and membranes were used in each experiment. The electrophoretic separation experiments were carried out under various conditions, including the ratio of the flowrate of dilute stream (Q_D, mL min^{-1}) to influent (Q_0, mL min^{-1}) ($q_d = Q_D/Q_0$), applied voltage, particle size, and initial particle concentration. Q_0 was fixed at 50 mL/min while q_d was varied between 0.1 and 0.9, which corresponded to the flow rate of the dilute stream ranging from 5 to 45 mL/min, or hydraulic retention time (HRT, min) of 1.8–0.2 min, respectively. The applied potential was adjusted within the range of 0–40 V, creating electric field strength (E) from 0 to 80 V cm^{-1}. The threshold of applied potential was 40 V considering the energy efficiency and work safety. The particle size of PS was between 300 and 1000 nm and the initial particle concentration ranged from 5 to 45 mg L^{-1}. The electrophoretic separation system was operated continuously at 10 min, or 20 HRT, which was adequate for steady-state condition (Fig. S4). Afterwards, the dilute stream was collected to analyze the concentration of submicron plastics particles using a turbidity meter (2100 P, Hach, Colorado, U.S.A.); effluent pH and conductivity were monitored by a pH meter (Accumet AE150, Thermo Fisher Scientific Inc., Maryland, U.S.A.) and a conductivity meter (CTSTestr 50 P, Oakton, South Carolina, U.S.A.), respectively. To verify the consistency of results, we have conducted two separate runs under identical conditions. As shown in Fig. S5, the difference in removal efficiency between two separate runs was minimal, confirming the reproducibility of the results.

3. Results and discussion

3.1. Theoretical aspect of particle movement in electrophoretic separator

The electrophoretic separation system relies on the migration of charged particles in an electric field. Fig. 2 shows the zeta potential of PS

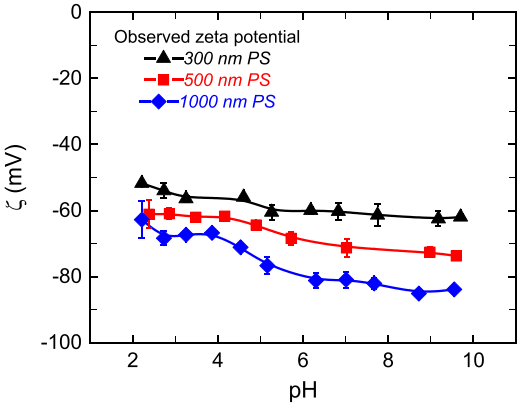

Fig. 2. Zeta potential (ζ) of PS latex as a function of pH. Experimental conditions: particle size d = 300–1000 nm, I = 10^{-3} M $NaClO_4$, number concentration = 5×10^{11} #/L.

latex, the model submicron plastics particles, as a function of pH. The PS particles were negatively charged over a wide range of pH, which is attributable to the deprotonation of surface sulfonate group, the surface defects caused by the initiator of polymerization process (Lin et al., 2023). As a strong Brȍnsted acid site, pH did not alter the degree of deprotonation of the sulfonate group, thereby resulting in a relatively flat zeta potential profile over the pH range of 2–10. Note that the zeta potential of PS particles became more negative as the particle size increased from 300 nm to 1000 nm. The average zeta potential was −56, −65, and −71 mV for particle size of 300, 500, and 1000 nm, respectively. With such negative zeta potential, the repulsive electrostatic force between particles would retard aggregation [20]. PS particles were stable in 10^{-3} M $NaClO_4$, as the Z-average size was measured as 311 ± 24, 511 ± 7, and 982 ± 150 nm for 300, 500, and 1000 nm PS latex, respectively, with polydispersity index below 0.1 [21]. The electrophoretic mobility (u_e, $m^2\ V^{-1}\ s^{-1}$) can be estimated based on the classic electrophoresis theory (Eq. 1) including a correction factor, f(α, ζ), to account for the deformation of both electric field and electrical double layer (EDL) [21]. As detailed in section S2 (Supporting Information), f(α, ζ) is greatly influenced by the particle radius relative to double layer thickness (α), which is the product of particle radius (R, m) and the reciprocal thickness of EDL (κ, m^{-1}). At low zeta potential ($|\zeta| <$ 25.7 V), f(α, ζ) varies from 1 when double layer is relatively thick (α < 0.1) to 1.5 when double lay is relatively thin (α > 100). At great zeta potential, the relaxation of electrical double layer is significant, causing f (α, ζ) to first decrease followed by increase. The electrophoretic velocity (v_e, m sec^{-1}) is related to mobility (u_e) and electric field (E) (Eq. 2).

$$u_e = \frac{2\varepsilon\varepsilon_0\zeta}{3\eta} f(\alpha,\zeta) \tag{1}$$

$$v_e = u_e E = \frac{2\varepsilon\varepsilon_0\zeta f(\alpha,\zeta)E}{3\eta} \tag{2}$$

The movement of particles in the separation chamber is controlled by the electrophoretic force and drag force. The flow is assumed to be completely mixed in the x and y direction but varied along the z direction. Water permeates through the membrane at a horizontal water velocity (v_w, m s^{-1}) that generates the dilute stream through an active permeation area (A, m^2) (Eq. 3). With mass balance on water flow (Supporting Information, section S3), the relationship between vertical water velocity (v_z, m s^{-1}) and position z is established as Eq. 4. As shown in Fig. 1b, the velocity of plastics particles is the resultant of v_w and v_z in the absence of an electric field. When an electric field is applied, v_e with a direction opposite to v_w is produced (Eq. 2); the velocity of plastics particles is the resultant of three velocities. At a given electric field strength, v_e is determined (Eq. 2); subtraction of v_e from v_w gives the horizontal terminal velocity (v_x, m s^{-1}) (Eq. 5). The critical electric field (E_c, V cm^{-1}) is defined when the horizontal terminal velocity is zero, i.e., $v_e = v_w$. Under such circumstance, electrophoresis prevents submicron plastics particles from permeating through the membrane to achieve complete particle removal. Eq. 6 allows the estimation of E_c, which is a function of v_w, ζ, and f(α, ζ). Note that Eq. 6 also implies that E_c is an operational function of dilution flow rate ($Q_d = Q_o q_d$), cell geometric dimension, such as H and L.

$$v_w = \frac{Q_D}{A} = \frac{Q_0 q_d}{HL} \tag{3}$$

$$v_z = v_{z0} - \frac{v_w z}{W} \tag{4}$$

$$v_x = v_w - v_e = v_w - u_e E \tag{5}$$

$$E_c = \frac{v_w}{u_e} = \frac{3\eta v_w}{2\varepsilon\varepsilon_0\zeta f(\alpha,\zeta)} = \frac{3\eta}{2\varepsilon\varepsilon_0\zeta f(\alpha,\zeta)} \frac{Q_0 q_d}{HL} \tag{6}$$

The electrophoretic separation of submicron plastics particles was run at ionic strength of 10^{-3} M $NaClO_4$ and different q_d values ranging from 0.5 to 0.9, which corresponded to Q_D from 25 to 45 mL/min at a constant Q_0 of 50 mL/min. Fig. 3 presents the variation in E_c as a function of particle size, zeta potential, and q_d. Results revealed that smaller q_d and more negative zeta potential lead to lower E_c. The results clearly indicate that as q_d decreases, v_w decreases and a lower E_c is sufficient to overcome the drag force of the permeation flow. Likewise, a more negative zeta potential results in a larger electric force due to the Columb's law. Hence, E_c is directly proportional to q_d and inversely proportional to the absolute value of zeta potential. Fig. 3 also shows that E_c gradually decreases to a constant value as the particle size increases, which is attributed to the effect of particle size on f(α, ζ) due to the distortion of electric field and EDL relaxation [22].

3.2. Electrophoretic separation of submicron plastics particles

3.2.1. Effect of hydraulic condition

The removal of 500-nm PS particles by the electrophoretic separation system was evaluated under various hydraulic conditions. With Q_0 of 50 mL min^{-1}, a wide range of electric field was tested at q_d between 0.5 and 0.9. The symbols in Fig. 4 and Fig. S6 were the observed removal while the lines were the simulations based on the model calculation (see next section). In the absence of an external electric field, i.e., $E/E_c = 0$, the removal efficiency was below 8 % due to inefficient rejection of 500 nm PS particles by membrane having a pore size of 10 μm. The presence of electric field enhanced the removal efficiency (Fig. S6). At given electric field, MPs removal decreased with increase in q_d. As q_d increased from 0.5 to 0.9, v_w increased from 0.29 to 2.57 cm/min, resulting in an increase in E_c from 60 to 108 V cm^{-1} according to Eq. 6. When the applied electric filed is normalized to E/E_c (Fig. 4), the removal at various q_d shows similar trends: particle removal increased with E/E_c and reached a plateau at $E/E_c \geq 1$. In theory, the electrophoretic velocity of PS particles at $E \geq E_c$ can offset the drag velocity of water flow, preventing PS particles from passing through the membrane into the dilute stream thus leading to complete particle removal. Nevertheless, there was notable deviations between observed and theoretical removal at $q_d > 0.7$ when $E/E_c > 0.7$. The removal plateaued at 70 % at q_d reaching 0.7 and 0.8. As q_d increased to 0.7, the flowrate of concentrate stream decreased dramatically, thereby hindering the removal of oxygen bubbles attached to membrane. Oxygen bubbles attachment to membrane reduced the active permeation area (A in Eq. 3) and leading to an increase in v_w. In other words, the actual E_c could be greater than the apparent E_c due to the inability to sustain active permeation area at $q_d > 0.7$ due to elevated applied potential requirement.

The pH and conductivity of the dilute stream were plotted in Fig. S7. Both pH and conductivity increased with increase in E/E_c. The applied voltage surpassed the hydrogen overpotential voltage [23]. Specifically, the water reduction occurred at the cathode, generating hydrogen gas and hydroxide ion the dilute stream, thereby increasing the solution pH and conductivity (Eq. 8). Although the pH of the influent was nearly neutral, significant increase in pH and conductivity was observed once the electric field was applied (Fig. S7). The overall energy consumption of the electrophoretic separation system could be readily justified by collection and use of H_2 and O_2 as hydrogen fuel and oxidation of organic or inorganic contaminants in water and wastewater treatment, respectively [24,25].

$$2H_2O + 2e^- \rightarrow H_2(g) + 2OH^- \tag{8}$$

3.2.2. Effect of particle size and initial concentration

The electrophoretic separation of PS particles with size from 300 to 1000 nm was investigated. As the zeta potential of PS particles of larger size was more negative (Fig. 2), E_c decreases accordingly (Eq. 6). The E_c of 100, 300, and 1000 nm PS particles are 115.7, 95.7, and 80.9 V cm^{-1}, respectively at q_d of 0.8. Fig. S8 shows that larger PS particles could be removed at lower electric field. After normalizing the electric field to E_c,

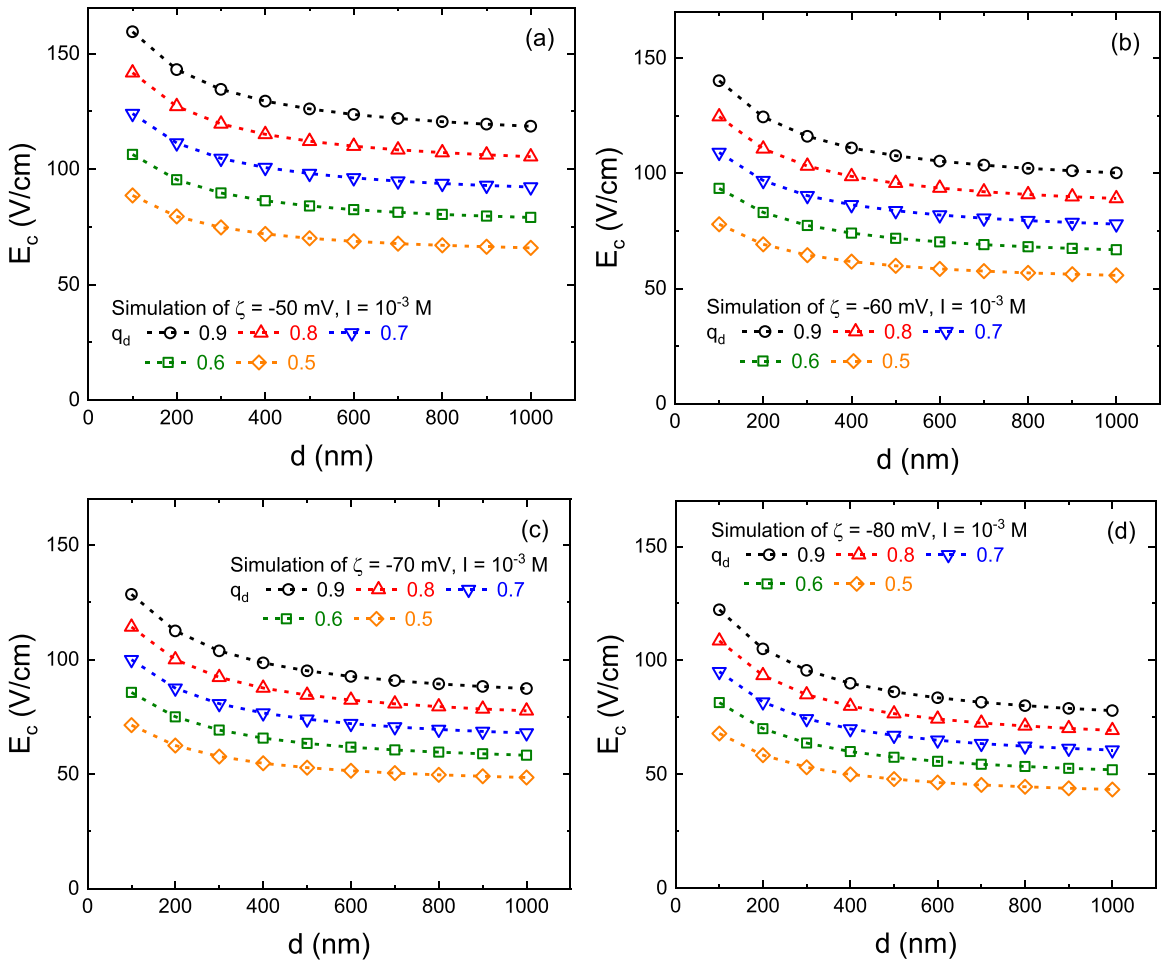

Fig. 3. Simulation of the critical electric field of particles with zeta potential of (a) −50 mV, (b) −60 mV, (c) −70 mV, and (d) −80 mV as a function of particle size in electrophoretic separation system.

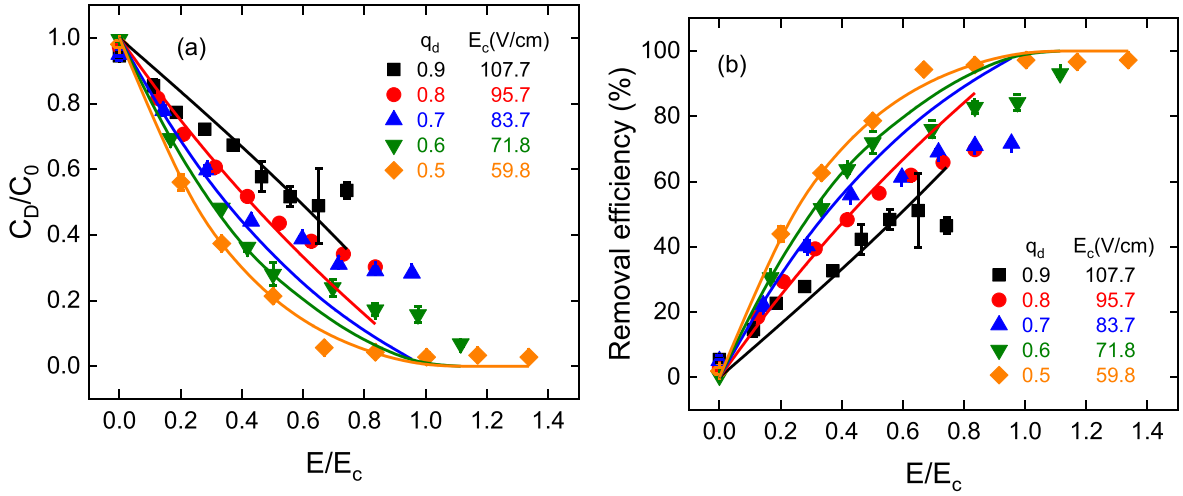

Fig. 4. Effect of hydraulic condition on (a) C_D/C_0 in dilute stream and (b) removal efficiency of PS particles as a function of E/E_c. (Q_0 = 50 mL/min, d = 500 nm, C_0 = 5 mg/L, I = 10^{-3} M $NaClO_4$).

Fig. 5a suggests the removal of PS particles with distinct size shared similar trends, suggesting that the electrophoretic separation was dominated by zeta potential and independent of particle size particle. The removal plateaued at 80 % near $E/E_c = 1$.

The effect of particle concentration on the removal of PS particles was investigated using 500- nm PS particles from 5 to 45 mg L^{-1}. As shown in Fig. 5b, the initial concentration did not affect the removal of PS particles significantly. At $q_d = 0.8$, the removal was around 70 % at $E = 80$ V cm^{-1} or $E/E_c = 0.84$. Generally, the removal appeared to be independent of particle concentration. Results implied that the finding

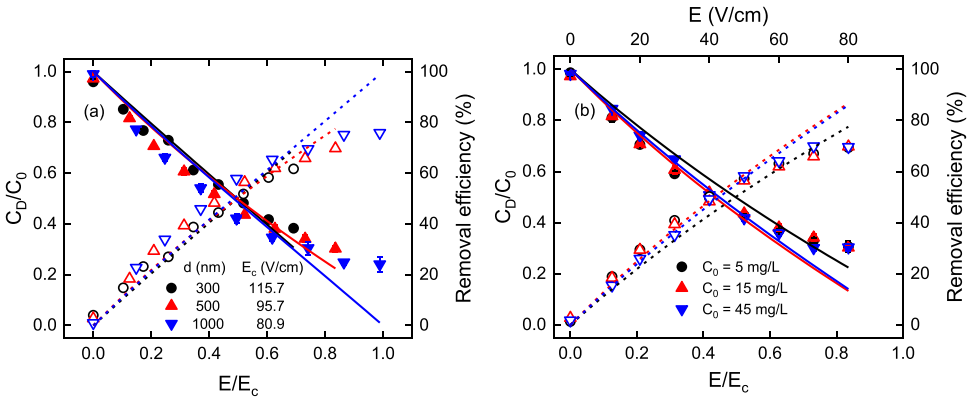

Fig. 5. Effect of (a) particle size and (b) initial concentration on C_D/C_0 and the removal of PS particles as a function of E/E_c. ($Q_0 = 50$ mL/min, d = 500 nm, $q_d = 0.8$, $C_0 = 5$ mg/L, $I = 10^{-3}$ M $NaClO_4$ unless stated otherwise.).

of this study can be readily applied to most surface waters containing lower concentrations of submicron plastics particles which is common in natural environment [26]. It is important to note that there is insignificant aggregation of PS particles during electrophoretic separation.

3.3. Modelling of electrophoretic separation

The removal efficiency of plastics particles in the electrophoretic separation system was analyzed based on mass balance and force acting on a single particle. To describe the transport and trajectories of submicron plastics particles in hydrodynamic and electrostatic field, the following assumptions were made: (1) the system is operated at steady state, *i.e.,* all variables are independent of time (2) the concentration of plastics particles only varies along z direction, (3) the active separation area (A) equals H•L and is independent of electric field, (4) v_w that passing through the membrane is uniform.

In the separation zone of electrophoretic cell, the terminal velocity of a single particle equals v_z and v_x in vertical and horizontal direction as shown Eq. 4 and Eq. 5, respectively. As shown in Fig. 1b, the direction and magnitude of v_x are related to the relative field strength, i.e., E/E_c. The fact that v_x is positive at $E < E_c$ suggests that plastics particles leave the concentration chamber at a flux (N_x, mg m^{-2} min^{-1}) of $C_z v_x$, where C_z is the concentration of plastics particles at height of z. At $E \geq E_c$, no plastics particles leave the concentration chamber because v_x is negative, i.e., $N_x = 0$. Under ideal situation where plastics particles do not attach on electrodes and membrane, the mass flowrate of plastics particles in influent ($\dot{m}_0$, mg min^{-1}) equals the sum of mass flowrates in concentrate and dilute streams, i.e., $\dot{m}_0 = \dot{m}_C + \dot{m}_D$. Unfortunately, such simplification cannot be applied as the deposition of plastics particles on anode and membrane occur frequently during electrophoretic separation. Electrostatic force is the major interactive force between plastics particles and electrode and membrane. When an electric field is applied, the anode is positively polarized that easily collects the negatively charged plastics particles. On the other hand, the stainless-steel membrane in electric field behaves as a bipolar electrode, i.e., an isolated conductor without direct electric connection while being polarized simultaneously [27]. Charge segregation resulted in the formation of cathodic pole at the concentration stream side and anodic pole at the dilute stream side. When the stream containing MPs passes through the polarized membrane, the deposition of negatively charged plastics particles on anodic pole occurred. The classical deposition model was applied to account for the particle deposition on both electrode and membrane. The rate of deposition of plastics particles on the anode and membrane (r_d, mg L^{-1} min^{-1}) is given by a pseudo-first-order rate reaction [28]:

$$r_d = -\frac{dC}{dt} = k_d C \tag{9}$$

$$k_d = \alpha_d \beta \tag{10}$$

where k_d is the pseudo-first-order rate constant (min^{-1}), which is a product of the dimensionless attachment probability (α_d) and the mass transport coefficient (β, min^{-1}). α_d is a function of the surface potential of the anode and the membrane, which increases with the applied potential, i.e., electric field. β is related to the hydraulic condition related to q_d. Consequently, mass balance on plastics particles in the electrophoretic separation system can be written as:

$$\dot{m}_0 = \dot{m}_C + \dot{m}_D + \dot{m}_A + \dot{m}_M \tag{11}$$

where $\dot{m}_0$, $\dot{m}_C$, and $\dot{m}_D$, are the mass flowrates (mg/min) of PS particles flowing into the reactor, out of the reactor in concentration stream and dilute stream, respectively. $\dot{m}_A$ and $\dot{m}_M$ are the mass deposition rate (mg/min) of plastics particles on the anode and the membrane, individually. Fig. S9 illustrates the distribution of plastics particles under three different scenarios in terms of applied field relative to the critical value. At E = 0, the entering particles are distributed to $\dot{m}_C$ and $\dot{m}_D$. When potential is applied, the electrode and membrane are polarized. At $E \geq E_c$, no plastics particles would permeate the membrane and thus all entering particles are either being deposited on anode ($\dot{m}_A$) or appeared in concentrate stream ($\dot{m}_C$). In the case that $0 < E \leq E_c$, certain amounts of particles would permeate the membrane, so some particles would be deposited membrane ($\dot{m}_M$) and appeared in the dilute stream ($\dot{m}_D$). As detailed in section S5 in Supporting Information, the mass flowrates are derived through a series mass balance in finite volume followed by integration. Tables 1 and 2 summarizes the concentration of plastics particles in dilute relative to initial concentration, as well as the mass flowrates and deposition rates.

Fig. 6 presents the mass flowrates of dilute stream ($\dot{m}_D$) and membrane deposition ($\dot{m}_M$), which sum gives the total removal of PS particles in the electrophoretic separation system. At E = 0 where no separation occurred, $\dot{m}_D$ equals the ratio of dilute to influent, q_d. The membrane deposition was negligible without applied potential, affirming that PS particles were not removed by size exclusion. As the applied potential increased, electrophoretic force would retard the flux of PS particle from passing through the membrane; the theoretical flux rate was modelled as blue lines in Fig. 6. Notably, the observed mass flowrate of dilute stream was smaller than that of the theoretical value due to the contribution of membrane deposition ($\dot{m}_M$). As E increased, the membrane would be polarized and become a collector of negatively-charged PS particle. The parabolic relationship between membrane deposition mass flowrate and E was the resultant of membrane deposition and electrophoretic separation. On one hand, the linear relation between deposition rate constant and E ($k_M = b \bullet E$, Eq. S34) suggests that the deposition rate increased dramatically with E. On the other hand, the electrophoresis model predicts that the permeation flux of PS particles declines with at

Table 1
List of symbols assignments and units.

Alphabet		
C	Concentration of particles	mg L^{-1}
C_0	Concentration of particles in influent	mg L^{-1}
C_D	Concentration of particles in dilutes stream	mg L^{-1}
C_z	Concentration of particles at position z	mg L^{-1}
E	Electric field	V cm^{-1}
E_c	Critical electric field	V cm^{-1}
I	Current	A
k_d	Deposition rate constant	s^{-1}
k_A	Pseudo anode deposition rate constant	s^{-1}
k_M	Membrane deposition rate constant	s^{-1}
L	Length of electrophoretic cell	m
N_x	Flux of MPs at x-direction	mg m^{-2} min^{-1}
N_z	Flux of MPs at z-direction	mg m^{-2} min^{-1}
$\dot{m}_0$	Influent mass flow rate of MPs	mg min^{-1}
$\dot{m}_A$	Mass deposition rate of MPs on anode	mg min^{-1}
$\dot{m}_C$	Effluent mass flow rate of MPs with concentrate stream	mg min^{-1}
$\dot{m}_D$	Effluent mass flow rate of MPs with dilute stream	mg min^{-1}
$\dot{m}_M$	Mass deposition rate of MPs on membrane	mg min^{-1}
Q	Volumetric flowrate	m^3 s^{-1}
q_d	Dilute-to-influent flow rate ratio	-
r_d	Deposition rate	mg L^{-1} min^{-1}
T	Thickness of membrane	m
u_e	Electrophoretic mobility	m^2 V^{-1} s^{-1}
V	Applied voltage	V
v_e	Electrophoretic velocity	m s^{-1}
v_w	Horizontal velocity of water passing through the membrane	m s^{-1}
v_x	Horizontal terminal velocity of particles	m s^{-1}
v_z	Vertical velocity of water and particles	V s^{-1}
W	Width of electrophoretic cell	m
z	Z-axis position	m
Greek		
α	Particle size relative to double layer thickness	-
α_d	Dimensionless attachment probability	min^{-1}
β	Dimensionless mass transport coefficient	-
δ	Thickness affected by anodic deposition	m
ε_0	Vacuum permittivity	C V^{-1} m^{-1}
ε_r	Relative permittivity	-
η	Dynamic viscosity	kg m^{-1} s^{-1}
κ	Reciprocal of double layer thickness	m^{-1}
ζ	Zeta potential	V

Table 2
Summary of modeled equations of concentration profile and mass flow rate of microplastics in the electrophoretic separation system.

	$E < E_c$	$E \geq E_c$
C_D/C_0	$\frac{e^{-k_M T/v_w}}{q_d}\left(\frac{-v_e+v_w}{k'_A W-v_e+v_w}\right)\left[1-(1-q_d)^{(k'_A W-v_e+v_w)/v_w}\right]$	0
$\dot{m}_0$	$C_0 Q_0$	$C_0 Q_0$
$\dot{m}_C$	$C_0 Q_0 (1-q_d)^{(k'_A W-v_e+v_w)/v_w}$	$C_0 Q_0 (1-q_d)^{k'_A W/v_w}$
$\dot{m}_D$	$C_0 Q_0 e^{-k_M T/v_w}\left(\frac{-v_e+v_w}{k'_A W-v_e+v_w}\right)\left[1-(1-q_d)^{(k'_A W-v_e+v_w)/v_w}\right]$	0
$\dot{m}_A$	$C_0 Q_0\left(\frac{k'_A W}{k'_A W-v_e+v_w}\right)\left[1-(1-q_d)^{(k'_A W-v_e+v_w)/v_w}\right]$	$C_0 Q_0\left[1-(1-q_d)^{k'_A W/v_w}\right]$
$\dot{m}_M$	$C_0 Q_0 (1-e^{-k_M T/v_w})\left(\frac{-v_e+v_w}{k'_A W-v_e+v_w}\right)\left[1-(1-q_d)^{(k'_A W-v_e+v_w)/v_w}\right]$	0

increase in E ($N_{x,z} = C_z v_x = C_z(v_w - v_e)$, Eq. S15). As a result, the $\dot{m}_M$ first increased with E due to enhanced deposition rate, then declined to zero as E approached E_c, where no PS particle should pass through the membrane. Therefore, the particle removal at $E > E_c$ was facilitated via electrophoresis without other contributions such as cake formation [19]. From the viewpoint of energy efficiency and MP deposition minimization, it is desirable to maintain the electric field strength at E_c to ensure the effective removal of submicron plastics particles while minimizing energy consumption at the same time.

3.4. Engineering aspect and cost analysis

3.4.1. Engineering aspect

A 6-h test on electrophoretic separation of PS particles was conducted to evaluate the stability in removal efficiency and identify possible deterioration mechanism. Fig. S9 presents the variation of C_D/C_0 and current over time at $E = 1.2E_c$. While the removal remained constantly high at 97 % throughout the experiment, the current gradually declined from 250 mA to 230 mA (~8 % loss). Since the operation was conducted at constant voltage, this decrement in current suggests an increase in total resistance increased, probably due to the deposition of PS MPs on anode. In other words, the increase in resistance at electrode/solution interface can cause a potential drop, reducing the effective electric field. Based on Ohm's law, the effective electric field is proportional to current density. At 6 h, the effective electric field was estimated to be 66.1 V cm^{-1} (~$1.1E_c$), which explains why the removal was unaffected. However, additional measures, such as periodic electrode reversal and mechanical cleaning, would be necessary to mitigate particles deposition on electrodes.

The lifespan of electrodes is influenced by three deterioration mechanisms: (1) particles deposition, (2) passivation, and (3) anodic dissolution. While the deposition of PS particles occurs, it can be mitigated through electrode reversal and mechanical cleaning. The passivation effect would be minimal in our system with $NaClO_4$ as the electrolyte, as evidenced in the constant current level during the prolonged test. The result suggests that the oxidized layer remains conductive enough to sustain the oxygen evolution reaction (OER). Although anodic dissolution of stainless-steel anode could release iron ions, which might lead to precipitates such as yellowish $Fe(OH)_3$ under specific conditions. However, there is no observed iron hydroxide or oxyhydroxide precipitates throughout the experiment in our system. Therefore, we expect that the lifespan of the electrodes used in this experiment ($NaClO_4$ as electrolyte) could be more than 1 year. However, if the influent contains elevated concentration of chloride or alkaline earth ions, the lifespan could be shorter. The chloride ion is known to promote anodic dissolution by forming iron-chloride complex, known as pitting corrosion [29]. The presence of alkaline earth ions and high alkalinity may cause carbonate precipitation at cathode due to localized high pH [30]. Taking these factors into account, the life span of electrodes may be reduced to 6 months.

For effective application in real-world freshwater, the electrophoretic separation system must consider the type of contaminant present in freshwater. Natural organic matters (NOMs) and metal ions could affect the performance of electrophoretic separation if being adsorbed on MPs. Since NOMs are generally negatively charged, their adsorption onto MPs is unlikely to alter the intrinsic negative zeta potential of MPs significantly. Hence, the effect of NOMs on electrophoretic separation of MPs is expected to be minimal. However, multivalent metal ions, such as alkaline earth metals (Ca^{2+} and Mg^{2+}) and trace heavy metals (Cu^{2+}, Pb^{2+}) could impair the electrophoretic removal. The specific adsorption of these multivalent metal ions could partially neutralize the negative surface charge of MPs, shifting the zeta potential to a less negative value. In that case, the electrophoretic mobility of MPs would decrease (Eq. 2) and the interparticle interaction could be relevant to induce aggregation. To maintain efficient electrophoretic removal of MPs in the presence of NOMs and metal ions, periodic zeta potential and size measurement of MPs would be recommended. This would allow accurate estimation of E_c (Eq. 6), which is necessary for adjusting the applied electric field accordingly.

3.4.2. Cost analysis

To evaluate the energy efficiency of the electrophoretic separation system, the specific energy consumption required per unit volume of

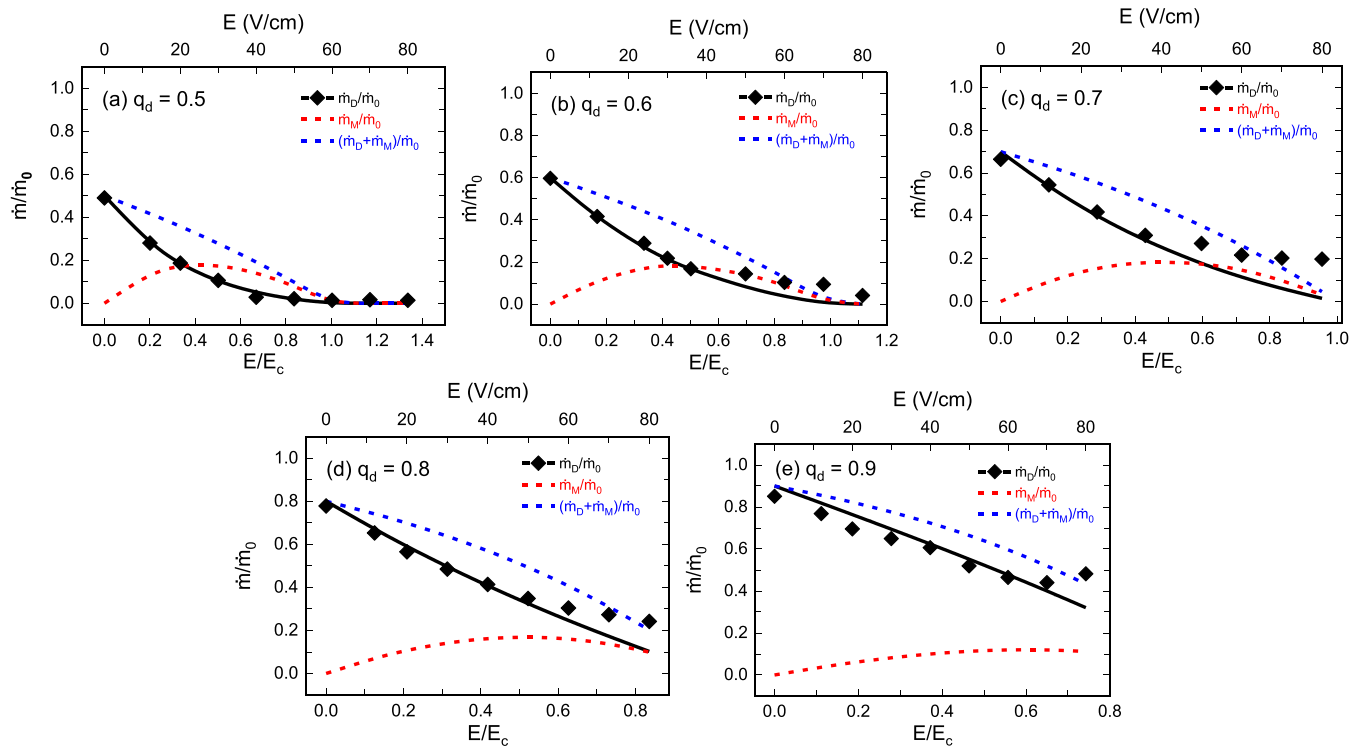

Fig. 6. Observed and simulated mass balance on PS particles in the electrophoretic separation system operated at q_d of (a) 0.5, (b) 0.6, (c) 0.7, (d) 0.8, (e) 0.9. (Q_0 = 50 mL/min, d = 500 nm, C_0 = 5 mg/L, I = 10^{-3} M $NaClO_4$).

dilute water production was calculated according to Eq. 12.

$$SEC = \frac{VI}{Q_D} \times 36000 \quad (12)$$

whereSEC is the specific energy consumption (kW m^{-3}-dilute water), V is the applied potential (V), I is the current (A), and Q_D is the flow rate of dilute stream (m^3 min^{-1}). Since maximal particle removal was accomplished near E_c, the E_c potential and corresponding current were used to calculate specific energy consumption. Fig. 7a shows that the specific energy consumption was 5.0, 5.6, and 8.6 kWh m^{-3} at q_d = 0.5, = 0.6, and = 0.9, respectively. Since E_c is proportional to q_d (Eq. 6), the specific energy consumption increases linearly with q_d. The specific energy consumption of electrophoretic separation system is compared with those conventional cross-flow filtration and eletrofiltration systems. The energy consumption of cross-flow filtration system was 1.4 – 3.5 kWh m^{-3} [31], 2.51 kWh m^{-3} [32], 8.59 kWh m^{-3} [33], and 3 ~ 8 kWh m^{-3} [34]. Wakeman and Sabri have reported an energy consumption of ~ 2.5 kWh m^{-3} for the cross-flow microfiltration of titania suspensions using pulsed electric field [35]. Hsieh et al. have studied electro-ultrafiltration for the removal of arsenic from groundwater and reported an energy consumption of ~ 4 kWh m^{-3} [36]. The energy demand of the electrophoretic separation system in this study was 5.0 ~ 8.6 kWh m^{-3}, which was comparable to values reported in the literature. In conclusion, the electrophoretic separation system was economically viable for the removal of submicron plastics particles from water.

Fig. 7b and c present the effect of particle size (zeta potential) and initial concentration on specific energy consumption for the electrophoretic separation of submicron plastics PS particles, respectively. The specific energy consumption at q_d = 0.8 was evaluated at the plateaued removal of 70 %. As shown in Fig. 7b, the specific energy consumption decreased with increasing particle size. Obviously, the electrophoretic mobility, i.e., zeta potential (ζ), was the dominant factor of energy consumption. Since the zeta potential became more negative as the size of PS particles increased, smaller electric field and energy consumption are required to remove larger PS particles. Consequently, the specific energy consumption is inversely linear with the larger PS particles. On the other hand, the ζ potential of PS particle was invariant with the particle concentration, resulting in negligible difference with respect to the specific energy consumption during the electrophoretic removal (Fig. 7c). The specific energy consumption was 5.06 ± 0.08 kWh m^{-3}.

The operation and maintenance cost (O&M cost) of electrophoretic separation system was evaluated. As detailed in S6 in supporting information, the annual O&M cost of electrophoretic was estimated considering electricity, material, and labor cost. For the sake of simplicity, a preliminary O&M const could be assessed for an electrophoretic separation system with an active separation area of 1 m^2, dilute stream production rate of 1368 L m^{-2} h^{-1} under optimal condition (q_d = 0.8) and generating 11,440 m^3 dilute stream per year. Based on a specific energy consumption of 5 kWh m^{-3} and electricity price of 0.086 USD/kWh, the annual electricity cost totals USD 4902/yr. The replacement of stainless-steel electrodes and membrane twice per year costs USD 50/yr. The regular manual maintenance cost (8 labor hours per month at an hourly rate of USD 5.76 in Taiwan) is estimated at USD 553/yr. Therefore, the annual O&M cost would be USD 5505/yr, equivalent to a specific cost of USD 0.48/m^3. Note that the electricity accounts for 89 % of the O&M cost, followed by labor (10 %) and materials (1 %).

The cost-effectiveness of electrophoretic separation system was evaluated to compare with conventional MF process. As shown in Table S4, the cost of MF varies with system size. The annual O&M cost is relatively high at small scale, being 1.55 and 0.40 US$/$m^3$ at design flow of 38 and 380 cmd, respectively. However, as MF system scales exceed 3800 cmd, its O&M cost drops below that of the electrophoretic separation. In addition, the electrophoretic separation may also be more favorable when considering capital costs. As shown in Table S4, MF systems require high-pressure pumps and pressurized filtration modules, leading to substantial capital costs, particularly below 3800 cmd. In contrast, the electrophoretic system operates via an electric field rather than size exclusion, enabling the use of membranes with larger pores, thereby minimizing transmembrane pressure drop and reducing capital

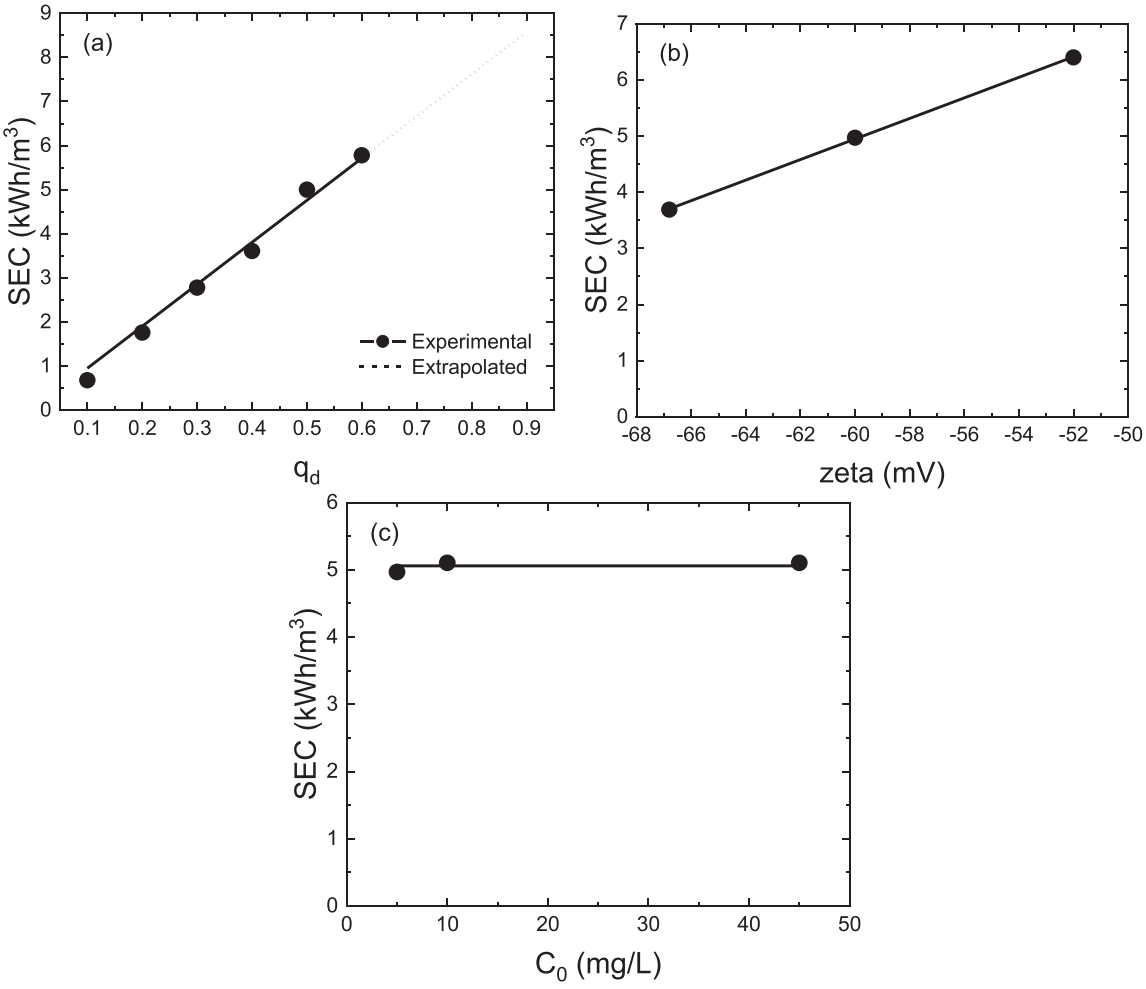

Fig. 7. Specific energy consumption (SEC) of electrophoretic removal of submicron plastics particles as affected by (a) hydraulic condition, (b) particle size, and (c) initial concentration.

expenses. In summary, the electrophoretic separation is more cost-effective than MF at small scales. It will be suitable for decentralized wastewater treatment facilities, especially those powered by renewable energies to utilize the generated DC current for water purification.

4. Conclusion

An electrophoresis separation system was designed and operated to remove submicron plastics particles from aqueous solution, exemplified by PS plastics nanoparticles. The intrinsic negative surface charge of plastics surface enables the generation of an electrostatic force counterbalance the drag force of water flow to produce a plastics-free dilute stream. The critical electric field (E_c), i.e., minimum electric field, for high degree particle separation, was dependent on hydraulic condition (i.e., water velocity, and cell volume), size and zeta potential of PS particles. The experimental results confirmed that electrophoresis was the primary mechanism of PS particles removal with efficiency being controlled by the relative applied electric field, i.e., E/E_c. An electric field greater than E_c was essential to produce plastics-free dilute stream. A mathematical model based on electrophoresis and particle mass balance described well the efficiency of MPs as a function hydraulic condition, electric field, zeta potential, and size of PS particles. The specific operation and maintenance cost of electrophoretic separation was estimated to be USD 0.48/m^3, which is more competitive than conventional MF at small scale. Therefore, the electrophoretic separation system shows great potential in decentralized wastewater treatment plants, particularly those powered by renewable energy. Further refinements of the reactor are underway in treating river water spiked with MPs as to validate the stability and scalability of the electrophoretic separation system.

CRediT authorship contribution statement

Hyunook Kim: Writing – review & editing, Funding acquisition, Conceptualization. **Chin-Pao Huang:** Writing – review & editing, Supervision, Conceptualization. **Cuijuan Feng:** Visualization, Formal analysis, Data curation. **Ingyu Lee:** Resources, Project administration. **JUI-YEN LIN:** Writing – review & editing, Writing – original draft, Investigation, Formal analysis, Data curation, Conceptualization.

Declaration of Competing Interest

The authors declare that they have no known competing financial interests or personal relationships that could have appeared to influence the work reported in this paper.

Acknowledgement

This work is supported by the National Research Foundation of Korea (NRF) in a grant funded by the Korea government (MSIT) (No. 2020R1A2C2101347) and the Graduate Program for Plastic-free Society funded by Korea Environmental Industry and Technology Institute.

Additional support was provided by the National Science and Technology Council, Taiwan, to Jui-Yen Lin, under contract No. MOST-110–2917-I-564–033 and NSTC 112–2222-E-992–009-MY2. H. Kim was supported by Graduate School Specializing in Plastic-free Society Funded by Korea Environmental and Industry Institute.

Appendix A. Supporting information

Supplementary data associated with this article can be found in the online version at doi:10.1016/j.jece.2024.115010.

Data availability

Data will be made available on request.

References

[1] J. Zheng, S. Suh, Strategies to reduce the global carbon footprint of plastics, Nat. Clim. Change 9 (2019) 374–378, https://doi.org/10.1038/s41558-019-0459-z.
[2] O.S. Alimi, J. Farner Budarz, L.M. Hernandez, N. Tufenkji, Microplastics and nanoplastics in aquatic environments: aggregation, deposition, and enhanced contaminant transport, Environ. Sci. Technol. 52 (2018) 1704–1724, https://doi.org/10.1021/acs.est.7b05559.
[3] M. Enfrin, L.F. Dumée, J. Lee, Nano/microplastics in water and wastewater treatment processes – Origin, impact and potential solutions, Water Res 161 (2019) 621–638, https://doi.org/10.1016/j.watres.2019.06.049.
[4] M. MacLeo, H.P.H. Arp, M.B. Tekman, A. Jahnke, The global threat from plastic pollution, Science 373 (2021) 61–65, https://doi.org/10.1126/science.abg5433.
[5] H. Cai, E.G. Xu, F. Du, R. Li, J. Liu, H. Shi, Analysis of environmental nanoplastics: progress and challenges, Chem. Eng. J. 410 (2021) 128208, https://doi.org/10.1016/j.cej.2020.128208.
[6] D.M. Mitrano, P. Wick, B. Nowack, Placing nanoplastics in the context of global plastic pollution, Nat. Nanotechnol. 16 (2021) 491–500, https://doi.org/10.1038/s41565-021-00888-2.
[7] J. Gigault, H. El Hadri, B. Nguyen, B. Grassl, L. Rowenczyk, N. Tufenkji, S. Feng, M. Wiesner, Nanoplastics are neither microplastics nor engineered nanoparticles, Nat. Nanotechnol. 16 (2021) 501–507, https://doi.org/10.1038/s41565-021-00886-4.
[8] V.S. Koutnik, S. Alkidim, J. Leonard, F. DePrima, S. Cao, E.M.V. Hoek, S. K. Mohanty, Unaccounted microplastics in wastewater sludge: where do they go? ACS EST Water 1 (2021) 1086–1097, https://doi.org/10.1021/acsestwater.0c00267.
[9] J. Hwang, D. Choi, S. Han, S.Y. Jung, J. Choi, J. Hong, Potential toxicity of polystyrene microplastic particles, Sci. Rep. 10 (2020) 7391, https://doi.org/10.1038/s41598-020-64464-9.
[10] R. Nugnes, M. Lavorgna, E. Orlo, C. Russo, M. Isidori, Toxic impact of polystyrene microplastic particles in freshwater organisms, Chemosphere 299 (2022) 134373, https://doi.org/10.1016/j.chemosphere.2022.134373.
[11] Y. Zhang, X. Wang, Y. Li, H. Wang, Y. Shi, Y. Li, Y. Zhang, Improving nanoplastic removal by coagulation: impact mechanism of particle size and water chemical conditions, J. Hazard. Mater. 425 (2022) 127962, https://doi.org/10.1016/j.jhazmat.2021.127962.
[12] I. Ali, X. Tan, Y. Xie, C. Peng, J. Li, I. Naz, Z. Duan, P. Wan, J. Huang, J. Liang, Z. Rui, Y. Ruan, Recent innovations in microplastics and nanoplastics removal by coagulation technique: implementations, knowledge gaps and prospects, Water Res 245 (2023) 120617, https://doi.org/10.1016/j.watres.2023.120617.
[13] S. Frehland, R. Kaegi, R. Hufenus, D.M. Mitrano, Long-term assessment of nanoplastic particle and microplastic fiber flux through a pilot wastewater treatment plant using metal-doped plastics, Water Res 182 (2020) 115860, https://doi.org/10.1016/j.watres.2020.115860.
[14] J. Talvitie, A. Mikola, A. Koistinen, O. Setälä, Solutions to microplastic pollution–Removal of microplastics from wastewater effluent with advanced wastewater treatment technologies, Water Res 123 (2017) 401–407, https://doi.org/10.1016/j.watres.2017.07.005.
[15] B. Ma, W. Xue, C. Hu, H. Liu, J. Qu, L. Li, Characteristics of microplastic removal via coagulation and ultrafiltration during drinking water treatment, Chem. Eng. J. 359 (2019) 159–167, https://doi.org/10.1016/j.cej.2018.11.155.
[16] M. Enfrin, J. Lee, P. Le-Clech, L.F. Dumée, Kinetic and mechanistic aspects of ultrafiltration membrane fouling by nano- and microplastics, J. Membr. Sci. 601 (2020) 117890, https://doi.org/10.1016/j.memsci.2020.117890.
[17] J.-Y. Lin, I. Lee, J.-H. Tzeng, W. Li, H. Kim, C.-P. Huang, The Surface acidity of freshly synthesized microplastics particles in simple electrolyte, Colloids Surf. Physicochem. Eng. Asp. 675 (2023) 132000, https://doi.org/10.1016/j.colsurfa.2023.132000.
[18] Y.-T. Lin, M. Sung, P.F. Sanders, A. Marinucci, C.P. Huang, Separation of nano-sized colloidal particles using cross-flow electro-filtration, Sep. Purif. Technol. 58 (2007) 138–147, https://doi.org/10.1016/j.seppur.2007.07.035.
[19] M. Sung, C.P. Huang, Y.-H. Weng, Y.-T. Lin, K.-C. Li, Enhancing the separation of nano-sized particles in low-salt suspensions by electrically assisted cross-flow filtration, Sep. Purif. Technol. 54 (2007) 170–177, https://doi.org/10.1016/j.seppur.2006.09.001.
[20] G.V. Lowry, R.J. Hill, S. Harper, A.F. Rawle, C.O. Hendren, F. Klaessig, U. Nobbmann, P. Sayre, J. Rumble, Guidance to improve the scientific value of zeta-potential measurements in nanoEHS, Environ. Sci. Nano 3 (2016) 953–965, https://doi.org/10.1039/C6EN00136J.
[21] J.-Y. Lin, I. Lee, C. Feng, H. Kim, C.-P. Huang, Electrophoresis characterization of nanoplastic particle surface charge in dilute aqueous electrolytes, Environ. Eng. Sci. (2024), https://doi.org/10.1089/ees.2024.0076.
[22] R.J. Hunter, Chapter 3 - The calculation of zeta potential, in: R.J. Hunter (Ed.), Zeta Potential Colloid Sci., Academic Press, 1981: pp. 59–124.
[23] G.C.C. Yang, T.-Y. Yang, S.-H. Tsai, Crossflow electro-microfiltration of oxide-CMP wastewater, Water Res 37 (2003) 785–792, https://doi.org/10.1016/S0043-1354(02)00388-3.
[24] M. Hakimhashemi, A.Y. Gebreyohannes, H. Saveyn, P. Van der Meeren, A. Verliefde, Combined effects of operational parameters on electro-ultrafiltration process characteristics, J. Membr. Sci. 403–404 (2012) 227–235, https://doi.org/10.1016/j.memsci.2012.02.054.
[25] Y.-H. Weng, K.-C. Li, L.H. Chaung-Hsieh, C.P. Huang, Removal of humic substances (HS) from water by electro-microfiltration (EMF), Water Res 40 (2006) 1783–1794, https://doi.org/10.1016/j.watres.2006.02.028.
[26] Z. Liu, M. Cai, D. Wu, P. Yu, Y. Jiao, Q. Jiang, Y. Zhao, Effects of nanoplastics at predicted environmental concentration on Daphnia pulex after exposure through multiple generations, Environ. Pollut. 256 (2020) 113506, https://doi.org/10.1016/j.envpol.2019.113506.
[27] A. Eden, K. Scida, N. Arroyo-Currás, J.C.T. Eijkel, C.D. Meinhart, S. Pennathur, Discharging behavior of confined bipolar electrodes: coupled electrokinetic and electrochemical dynamics, Electrochim. Acta 330 (2020) 135275, https://doi.org/10.1016/j.electacta.2019.135275.
[28] W. Stumm, J.J. Morgan. Aquatic Chemistry: Chemical Equilibria and Rates in Natural Waters, third edition, John Wiley & Sons, New York, 1995.
[29] F. Widhiastuti, J.-Y. Lin, Y.-J. Shih, Y.-H. Huang, Electrocoagulation of boron by electrochemically co-precipitated spinel ferrites, Chem. Eng. J. 350 (2018) 893–901.
[30] J. Luo, Z. Zhan, Y. Lei, Enhanced electrochemical softening of cooling water with three-dimensional cathodes, Desalination 577 (2024) 117405, https://doi.org/10.1016/j.desal.2024.117405.
[31] A. Jokić, I. Pajčin, J. Grahovac, N. Lukić, J. Dodić, Z. Rončević, Z. Šereš, Improving energy efficiency of Bacillus velezensis broth microfiltration in tubular ceramic membrane by air sparging and turbulence promoter, J. Chem. Technol. Biotechnol. 95 (2020) 1110–1115, https://doi.org/10.1002/jctb.6295.
[32] M.L. Gerardo, M.A. Zanain, R.W. Lovitt, Pilot-scale cross-flow microfiltration of *Chlorella minutissima*: a theoretical assessment of the operational parameters on energy consumption, Chem. Eng. J. 280 (2015) 505–513, https://doi.org/10.1016/j.cej.2015.06.026.
[33] J. Chamberland, D. Mercier-Bouchard, I. Dussault-Chouinard, S. Benoit, A. Doyen, M. Britten, Y. Pouliot, On the use of ultrafiltration or microfiltration polymeric spiral-wound membranes for cheesemilk standardization: impact on process efficiency, Foods 8 (2019) 198, https://doi.org/10.3390/foods8060198.
[34] S.D. Ríos, J. Salvadó, X. Farriol, C. Torras, Antifouling microfiltration strategies to harvest microalgae for biofuel, Bioresour. Technol. 119 (2012) 406–418, https://doi.org/10.1016/j.biortech.2012.05.044.
[35] R.J. Wakeman, M.N. Sabri, Utilizing pulsed electric-fields in cross-flow microfiltration of titania suspensions, Chem. Eng. Res. Des. 73 (1995) 455–463.
[36] L.-H.C. Hsieh, Y.-H. Weng, C.-P. Huang, K.-C. Li, Removal of arsenic from groundwater by electro-ultrafiltration, Desalination 234 (2008) 402–408, https://doi.org/10.1016/j.desal.2007.09.110.